Imaging of the Atomic Structure of All-Inorganic Halide Perovskites

Jeremy Hieulle[†,§], Shulin Luo[‡,§], Dae-Yong Son[†], Afshan Jamshaid[†], Collin Stecker[†], Zonghao Liu[†], Guangren Na[‡], Dongwen Yang[‡], Robin Ohmann[†,#], Luis K. Ono[†], Lijun Zhang[,‡], and Yabing Qi[*,†]*

[†]Energy Materials and Surface Sciences Unit (EMSSU), Okinawa Institute of Science and Technology Graduate University (OIST), 1919-1 Tancha, Onna-son, Okinawa 904-0495, Japan.

[‡]Key Laboratory of Automobile Materials of MOE and College of Materials Science and Engineering, Jilin University, Changchun 130012, China.

AUTHOR INFORMATION

Corresponding Authors

*(Yabing Qi: Yabing.Qi@OIST.jp). *(Lijun Zhang: lijun_zhang@jlu.edu.cn).

[#]Present Address: Department Physik, Universität Siegen, 57068 Siegen, Germany.

ABSTRACT. All-inorganic halide perovskites are promising materials for optoelectronic applications. The surface or interface structure of the perovskites plays a crucial role in determining the optoelectronic conversion efficiency, as well as the material stability. Thus far a thorough understanding of surface atomic structure of the inorganic perovskites and their contributions to their optoelectronic properties and stability is lacking. Here we show a scanning tunneling microscopy investigation on the atomic and electronic structure of $CsPbBr_3$ perovskite. Two different surface structures with a stripe and an armchair domain are identified, which originates from a complex interplay between Cs cations and Br anions. Our findings are further supported and correlated with density functional theory calculations and photoemission spectroscopy measurements. The stability evaluation of photovoltaic devices indicates a higher stability for $CsPbBr_3$ in comparison with $MAPbBr_3$, which is closely related to the low volatility of Cs from the perovskite surface.

TOC GRAPHICS

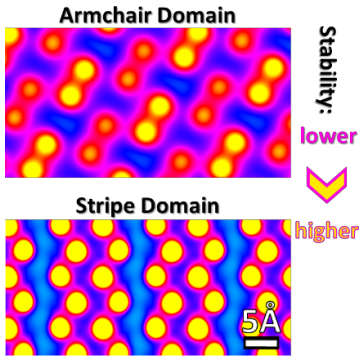

In the past few years, all-inorganic metal halide perovskites have attracted attention due to better stability and rapidly increasing performance,[1] making them suitable candidates for the development of high-performing optoelectronic devices with high stability.[2-9] For example, $CsPbBr_3$ was used to create highly sensitive x-ray and γ-ray detectors,[10] while $CsPbBr_3$ nanowires was employed to create high-quality laser cavities.[11-15] $CsPbBr_3$ was also used in the fabrication of stable light-emitting diodes (LEDs) with high purity green color.[16-18] Recently, the morphology and electronic properties of the interface layer of $CsPbBr_3$ perovskite have shown to play a crucial role in the optimization of the device performance.[19-22] Despite the clear influence of the interface, only a limited number of studies were performed to determine the structure of $CsPbBr_3$ perovskite surface and its influence on the material properties. A better knowledge of the $CsPbBr_3$ surface structure can enable more accurate band structure calculations, which can potentially lead to a better description of the interface properties in a device. A scanning transmission electron microscopy (STEM) study has shown that controlling the atomic packing at the grain boundary of $CsPbBr_3$ nanocrystals could enable a better control of the charge transfer at the interface between the perovskite and other layers in the device.[23] The high-angle annular dark field (HAADF) imaging by STEM relies on the atomic number of the element and does not allow observation of all the Br ions present at the surface due to the dominant signal of the Pb ions.[23] Therefore, a full picture of the atomic scale structure of the $CsPbBr_3$ surface is still lacking. Scanning tunneling microscopy (STM) is a powerful technique for determining the surface structure of perovskite materials with atomic scale precision.[24-27] Additionally, ultraviolet- and inverse photoemission spectroscopy (UPS-IPES) are useful tools to reveal the electronic structure of perovskite materials.[28-30]

Here, by combining STM, density functional theory (DFT) and UPS-IPES, we determine the exact structure of the inorganic $CsPbBr_3$ perovskite surface at the atomic scale and correlate it to the material electronic properties and stability. The objective of our research is to provide the explicit structural information of the inorganic perovskite surface/interface in order to provide a reliable basis for further in-depth understanding of the stability, charge transfer dynamics and other optoelectronic conversion related properties of the material. Our findings could potentially open new ways for engineering the inorganic perovskite device with tunable optoelectronic properties and high stability.

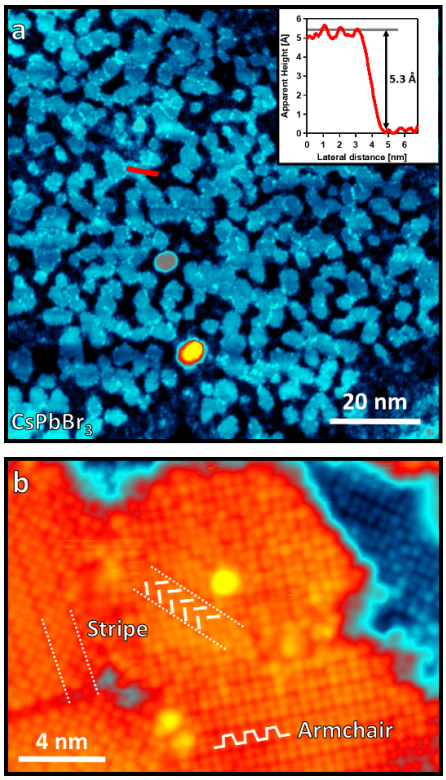

Figure 1 $CsPbBr_3$ surface topography. *(a) Large scale topographic image of the $CsPbBr_3$ film obtained by STM. Inset: profile taken along the red line in panel a, showing the step height of the perovskite material. (b) Magnified image of a). Two different reconstructions are observed at the surface of $CsPbBr_3$, a "stripe" domain and an "armchair" domain (indicated by the white segments in b). Image parameters: a) Bias = +3.0 V, Current = 22 pA, size = 96 × 96 nm^2; b) +2.0 V, 30 pA, size = 20 × 14.5 nm^2.*

The $CsPbBr_3$ perovskite films were grown on a clean Au(111) surface by dual source evaporation using CsBr and $PbBr_2$ precursor molecules in an ultra-high vacuum ($<10^{-9}$ Torr) environment (see Methods). Ultra-thin films with a thickness of about 4 ± 1 nm were prepared. The perovskite surface is atomically flat as can be seen in the STM image (Figure 1a), following a layer by layer growth mode. The top most layer is composed of interconnected grains with average diameter of 10 nm. The height of the islands is 5.3±0.3 Å (inset, Figure 1). In Figure 1b, a STM image with atomic resolution is shown. A close look at the topographic images reveals that the surface is composed of bright protrusions that are associated with bromine ions of the (010) surface of $CsPbBr_3$, as will be shown later. This surface atomic layer contains also Cs, however Cs cations are not resolved in the STM topography images due to their lower density of states compared to the Br anions. The Br anions form pairs that are periodically arranged. Two distinct domains can be observed at the surface of the $CsPbBr_3$ perovskite depending on the specific arrangement of the Br pairs (stripe and armchair domain in Figure 1b). The two domains occur in four different surface directions rotated by ±45°, ±90° with respect to each other (Figure S1). In Figure 1b a domain boundary between the stripe and armchair domains is resolved. At the boundary several defects occur, while the domains themselves are nearly defect free.

To understand the origin of the two distinct $CsPbBr_3$ domains (i.e., stripe and armchair) observed by STM, we performed first-principles DFT based calculations. For modeling the perovskite surface, we employed the ground-state orthorhombic crystal structure with the *Pnma* space group (see Methods). We find that the best agreement between experiment and theory is obtained for the (010) surface, which has only Cs and Br ions. Our calculations show that the bright protrusions observed in the STM images are the Br anions of the top CsBr surface layer. The Cs ions were not visualized in STM images due to their lower density of states compared to Br. The

two domains we observe can now be explained by two different surface reconstructions of the (010) surface. The reconstructions occur due to the solid-vacuum interface.

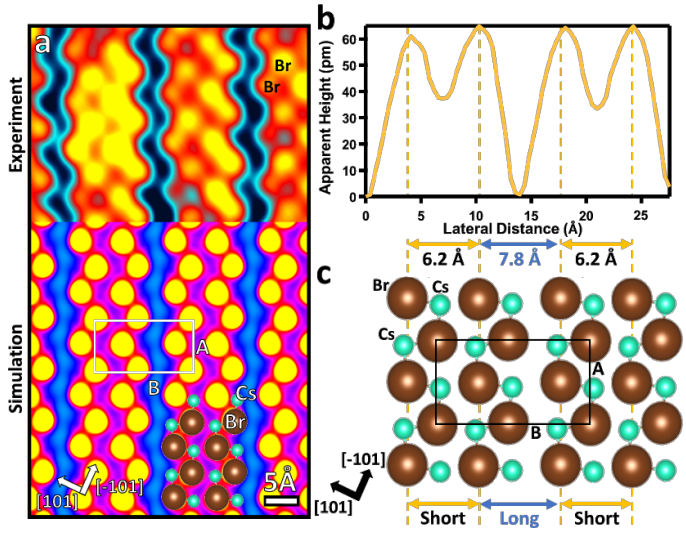

Figure 2. The stripe reconstruction of $CsPbBr_3$. (a) STM experimental image and simulated model. The white rectangle indicates the unit-cell of the stripe structure. (b) Line profile taken along the B vector of the unit-cell depicted in a. (c) Crystal structure model of the stripe domain, calculated by DFT. Brown balls represent Br ions, while green balls represent Cs ions. In the model the Br size have been artificially enlarged to highlight the Br pair formation (as observed in the experiment). The calculations show that the stripe structure originates from the alternation of short and long distance between neighboring Br pairs. Image parameters: a) Bias = +2.3 V, Current = 50 pA, size = 3.9 × 2.8 nm^2.

The stripe domain is depicted in Figure 2. The DFT calculations reproduce well the experimental STM images. The calculations show that the stripe domain of $CsPbBr_3$ originates from the alternation of short and long spacing between the Br pairs (Figure 2b-c), in accordance with the spacing measured experimentally. Within a stripe the Br pairs are separated by 6.2 Å (short spacing), while between two stripes the distance that separates the Br pairs is 7.8 Å (long spacing). The alternation of these two different spacing values is the main cause of the reconstruction. This reconstruction possesses a rectangular unit-cell with the following lattice parameters, A = 7.3 Å, and B = 14 Å (white rectangle, Fig. 2a). The surface unit cell is

composed of 4 Br^- and 4 Cs^+ ions (black square, Figure 2c). Our calculations reveal that the Br pairs are formed by Coulomb interaction between the Br^- and two Cs^+ cations placed nearby.

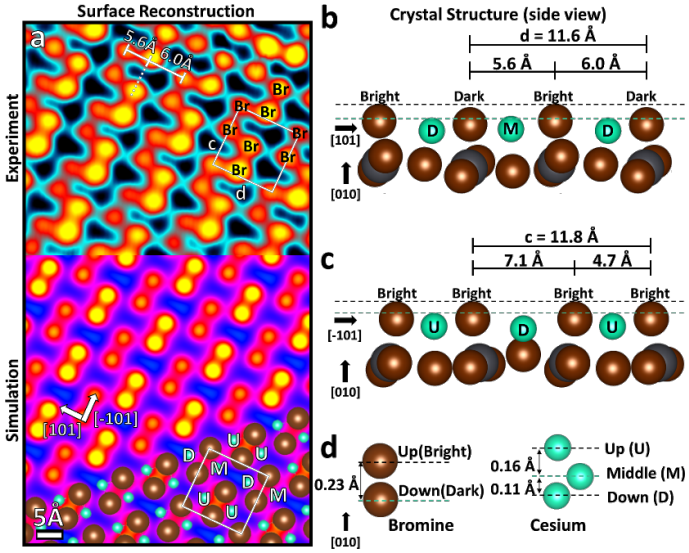

Figure 3. The armchair reconstruction of $CsPbBr_3$. (a) STM experimental image and superimposed simulated model. The white square represents the unit-cell of the armchair structure. (b-d) Side view of the calculated $CsPbBr_3$ armchair structure. Brown balls represent Br ions, while green balls represent Cs ions. In the model the Br size have been artificially enlarged to highlight the Br pair formation. The vertical positions of the Br and Cs ions are varying along the [101] direction, leading to the alternation of bright and dark rows in the experimental image. However, all the Br ions have the same vertical position in the [-101] direction (c). Br ions are found with two distinct vertical positions, while three positions are found for Cs ions (d). Image parameters: a) Bias = +2.0 V, Current = 100 pA, size = 5.2 × 4.2 nm^2.

The armchair domain is depicted in Figure 3. The calculated STM image matches well the experimental one. The domain consists of the alternation of bright and dark rows of Br pairs. The bright and dark rows run along the [-101] direction of the sample. The armchair packing results from the uneven spacing between bright and dark rows along the [101] direction (5.6Å and 6.0Å). The calculations show that the bright and dark Br rows originate from a change in the vertical position of the surface ions (Figure 3b-d). In fact, two distinct vertical positions were determined for the Br^- anions with a 23 pm difference, consistent with the contrast change observed in the STM image (Figure 3a). This change in the Br position is accompanied by a modification of the

Cs^+ vertical position. Three different heights were determined for the Cs cations, labeled as up (U), middle (M) and down (D). The bright Br pairs are formed by the interaction with two surrounding Cs cations placed in an up vertical position. In contrast, the dark Br pairs result from the interaction with two Cs cations placed in a middle and down position respectively. The unit cell of the armchair structure is rectangular with the following lattice parameters: c = 11.8 Å, d = 11.6 Å (white rectangle, Figure 3a). The motif of the unit cell consists of one up Br pair and one down Br pair with two Cs cations placed in an up position, one Cs in a middle, and one Cs in a down position (bottom of Figure 3a). The unit cell of the armchair structure is composed of 4 Br anions and 4 Cs cations, as in the stripe domain. Our DFT calculations show that the armchair domain is slightly less energetically favorable than the more compact stripe domain (Table S1, supplementary). Particularly, the calculated surface energy of the armchair surface is 0.0583 J/m^2, higher than 0.0450 J/m^2 of the stripe surface. We find that the refined structure optimization with the strict convergence criterion drives the armchair surface to transform to the stripe surface. This finding is coherent with the experimental observation, where the armchair domain was found to be less abundant than the stripe domain on the perovskite surface. The calculated distance between consecutive CsBr and CsBr planes is 5.69 Å. This distance corresponds well to the observed step height of the islands (5.3±0.3 Å), thus these can be assigned to a single layer of perovskite.

In the following we compare the $CsPbBr_3$ atomic structure to the previously observed $CH_3NH_3PbBr_3$ structure,[24,27,31] which contains the $CH_3NH_3^+$ molecule at the A site of the ABX_3 perovskite structure instead of the Cs^+ ion. Both perovskites crystallize in the orthorhombic structure exposing the (010) surface. $MAPbBr_3$ (MA = CH_3NH_3) shows surface reconstructions,

which are explained by different orientations of the non-symmetric MA molecules which interact with the Br^- cage. In the reconstructions the Br^- ions are forming pairs and have all the same height (see Figure S2 in supporting information). For the spherically symmetric Cs^+ we would thus expect only one type of reconstruction, as any rotation of the Cs^+ ion would not lead to a different interaction with the surrounding Br^- ions. However, two distinct domains can be clearly identified in $CsPbBr_3$, with one (armchair domain) having even different heights of the Br^- ions, in contrast to the $MAPbBr_3$ surface. Protrusions with distinct heights have been observed previously for mixed halide perovskites, were the I^- and Cl^- had different heights compared to the Br^-.[31] However, in this previous study, the different heights were found to originate from the distinct chemical nature of the halides present at the surface (i.e. I^-, Cl^- and Br^-). In the case of $CsPbBr_3$, only one type of halide (Br^-) is present at the surface. Although the different reconstructions for $MAPbI_3$ can be electronically switched by applying a voltage pulse,[26] we did not observe such an effect for $CsPbBr_3$. The two different domains of $CsPbBr_3$ are thus more stable.

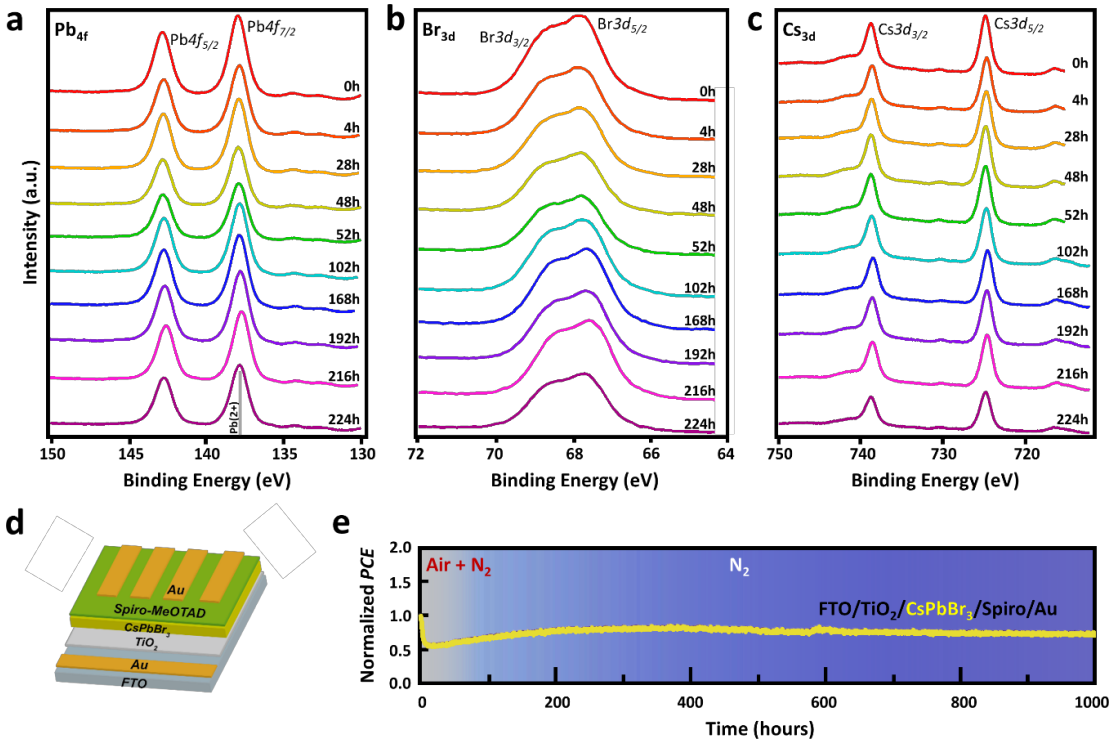

Figure 4. Stability check of $CsPbBr_3$ film and devices. (a-c) Evolution over time of the Pb *4f*, Br *3d* and Cs *3d* spectra of pristine $CsPbBr_3$, obtained by x-ray photoelectron spectroscopy (XPS) in an ultrahigh vacuum environment. (d) Device structure used for the stability test in e. (e) Evolution over time of the normalized power conversion efficiency (PCE) of a FTO/TiO_2/$CsPbBr_3$/spiro-OMeTAD/Au photovoltaic device. In both experiment (thin film in a-c, and device in d-e) a high stability of the $CsPbBr_3$ perovskite was observed.

All-inorganic perovskites have been reported to lead to a much higher device stability compared to its organic-inorganic counterpart.[1-5] However, at present it is not clear what is the origin of the high stability reported for those materials. Our objective is to get further insights in the fundamental origin of this high stability of all-inorganic perovskites. First, we performed a stability test by following the chemical evolution over time of the $CsPbBr_3$ film with XPS. Those measurements were performed in a well-controlled vacuum environment on a half-device architecture in order to get access to the intrinsic stability of the perovskite material, by excluding the influence of external factors such as humidity, or degradations related to the spiro-OMeTAD hole transport layer. The quality of the perovskite film used for the stability test was

confirmed by x-ray diffraction measurements (Figure S3). The evolution over time of the Pb *4f*, Br *3d* and Cs *3d* spectra of the $CsPbBr_3$ film are displayed in Figure 4 a-c respectively. Surprisingly, the XPS spectra appear to be almost unaltered over a period of 224h. This result contrasts with our previous study on the degradation of $MAPbBr_3$ perovskite film following a similar approach,[31] where a low degree of oxidation peak Pb(0) was found after only 4h in the vacuum chamber (Figure S4). The appearance of Pb(0) peak is the signature of the material degradation. Here the absence of such a peak after 224h under the beam, demonstrates the much better stability of $CsPbBr_3$ with respect to $MAPbBr_3$, in accordance with the previous reports on single crystal and thin film samples.[32] Additionally, X-ray beam damage was found to be minimal on a $MAPbBr_3$ reference sample (Figure S4b). The higher stability observed for $CsPbBr_3$ in a controlled vacuum environment without using any HTL suggests that the lower volatility of Cs species with respect to methylammonium significantly contributes to the superior stability of devices that use Cs-containing perovskite absorber layers. The higher stability observed for $CsPbBr_3$ with respect to $MAPbBr_3$ might also originate from the higher intrinsic stability of its two structural domains (i.e. armchair and stripe) as described earlier. This high intrinsic stability might prevent the desorption of the A cation in the photoactive material and thus explain the higher stability of devices based on all-inorganic $CsPbBr_3$ perovskite with respect to devices based on hybrid organic-inorganic $MAPbBr_3$ perovskite.

In order to check the stability in real device operation, using $CsPbBr_3$ films grown with the same protocol as for our XPS measurements, we followed the evolution of the power conversion efficiency (PCE) of a FTO/TiO_2/$CsPbBr_3$/spiro-OMeTAD/Au solar cell device, as a function of time (Figure 4d-e). A decrease of PCE was found during the first hour of operation, before it stabilizes to a reasonable value for over 1000 h under continuous operation. A typical current

density (J)-voltage (V) curve is given in Figure S5. Our measurements confirm the high stability of the $CsPbBr_3$ perovskite and are consistent with previous reports in the literature.

To get more insights on the electronic properties of $CsPbBr_3$ material we have performed ultraviolet- and inverse- photoemission spectroscopy on a 200 nm-thick $CsPbBr_3$ perovskite film grown on a c-TiO_2/FTO substrate *via* solution processing (see Methods). The $CsPbBr_3$ film was inserted in the vacuum chamber 24 h before the UPS and IPES measurements, in order to degas the sample thoroughly. The UPS and IPES data are plotted together in the top panel of Figure 5. Based on these results, we can determine that the bandgap is 2.3 eV, in good agreement with the previously reported value in the literature[28]. The measured bands were further compared to the calculated partial density of states (PDOS) of $CsPbBr_3$ perovskite, in the bottom panel of Figure 5. The PDOS was extracted from the atomic structure of the $CsPbBr_3$ armchair domain presented in Figure 3. The calculated PDOS reproduces well the valence and conduction band edges of the $CsPbBr_3$ perovskite film. We determined that the valence band (VB) near the Fermi level is mainly determined by the Br *4p* and Pb *6s* orbitals. In contrast, the main contributions to the conduction band (CB) come from the Pb *6p* and Br *4p* states. The Cs states lie at a much higher binding energy of ~7.4 eV with respect to the Fermi level (w.r.t. E_F) and does not contribute to the VB and CB edges near E_F (Figure S6). A 4.72 ± 0.20 eV work function was measured for the $CsPbBr_3$ film. This value is very close to the calculated work function of the $CsPbBr_3$ armchair and stripe domains (i.e., 4.72 and 4.73 eV respectively, table S1). To characterize the local electronic properties of the $CsPbBr_3$ perovskite we have also performed scanning tunneling spectroscopy (STS) on the vacuum deposited ultra-thin films presented in Figures 1-3. STS spectra are obtained by sweeping the bias voltage while recording the differential conductance (dI/dV) of the STM-sample junction. Such measurements allow determination of the local

density of states (LDOS) below the probe of the STM, with a lateral resolution down to the atomic level. The STS spectra obtained individually on the stripe and armchair domains are depicted in Figure S7. Surprisingly we find relatively similar electronic properties for both domains (i.e. stripe and armchair), despite their strong difference in term of structure. This is confirmed by the calculated PDOS of the two domains where only tiny differences can be observed (Figure S6). The local $CsPbBr_3$ bandgap measured by STS are in good agreement with the macroscopic UPS-IPES measurements (2.5 ± 0.2 eV). Our accurate band structure calculations were based on the precise atomic structure of the $CsPbBr_3$ surface determined by STM. Such precise determination of the band structure could allow a better prediction of the interfacial properties of $CsPbBr_3$ perovskite, and may open new ways for device engineering. A possible future step of our work, would be to use our model of the perovskite surface to perform accurate theoretical prediction of the charge transfer properties at the interface of $CsPbBr_3$ and an HTL or ETL layer in a device.

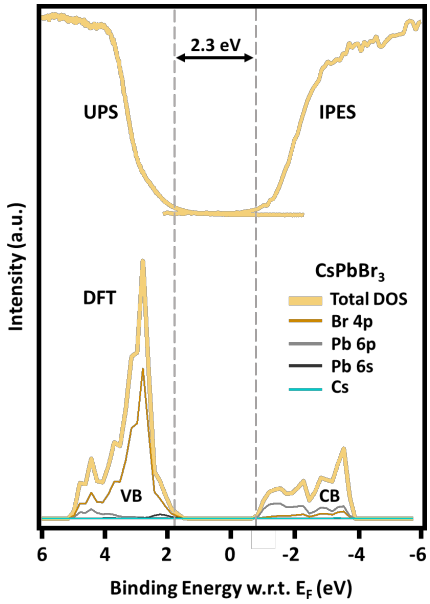

Figure 5. Valence and conduction bands of $CsPbBr_3$ perovskites. Top panel: Experimental ultra-violet and inverse photoelectron spectroscopy (UPS-IPES) spectra of pristine $CsPbBr_3$ perovskite. Bottom panel: Calculated PDOS of the $CsPbBr_3$ stripe domain. The thick curves represent the summation of all contributions of each orbital indicated by differently colored lines. The gray dashed line indicates the position of valence band and conduction band edges.

In this study, using STM measurements combined with DFT calculations, we identified two different structures on the surface of the $CsPbBr_3$ perovskite, a stripe domain and an armchair domain. The two surface structures originate from a complex interplay between the Cs cations and the Br anions. By performing a stability test on a half-device architecture in a well-controlled vacuum environment we get further insights into the origin of the high stability of all-inorganic perovskite with respect to its hybrid organic-inorganic counterpart. The high stability of $CsPbBr_3$ with respect to $MAPbBr_3$ is partly related to the lower volatility of the Cs species in comparison to the MA cation. Our study on the origin of the $CsPbBr_3$ exceptional stability could open new ways toward stable perovskite devices.

ACKNOWLEDGMENT

This work was supported by funding from the Energy Materials and Surface Sciences Unit of the Okinawa Institute of Science and Technology Graduate University, the OIST R&D Cluster Research Program, the OIST Proof of Concept (POC) Program, the JSPS KAKENHI Grant Number JP18K05266, and the Basic Science Research Program through the National Research Foundation of Korea (NRF) funded by the Ministry of Education (NRF-2018R1A6A3A03011234). The work at Jilin University was supported by the National Natural Science Foundation of China (Grants No. 61722403 and 11674121) and Jilin Province Science and Technology Development Program (Grant No. 20190201016JC). Calculations were performed in part at the high-performance computing center of Jilin University.

SUPPORTING INFORMATION

1. Energetics of the $CsPbBr_3$ systems estimated by DFT
2. Domain orientations at the $CsPbBr_3$ surface
3. Comparison of $MAPbBr_3$ versus $CsPbBr_3$ surfaces
4. XRD measurements of the 200 nm $CsPbBr_3$ films used in the stability check
5. Aging of a $MAPbBr_3$ reference sample followed by XPS
6. Device architecture and J-V curves
7. Full-range of the calculated PDOS
8. Scanning Tunneling Spectroscopy on $CsPbBr_3$
9. XPS curve fitting and chemical ratio
10. Methods

ORCID IDs

Jeremy Hieulle: 0000-0003-4891-4007
Dae-Yong Son: 0000-0001-6898-5326
Afshan Jamshaid: 0000-0001-5983-1544
Collin Stecker: 0000-0003-4247-5699
Zonghao Liu: 0000-0003-4743-6971
Robin Ohmann: 0000-0003-2483-1282
Luis K. Ono: 0000-0003-3176-1876
Lijun Zhang: 0000-0002-6438-5486
Yabing Qi: 0000-0002-4876-8049

REFERENCES

(1) Chen, J.; Morrow, D.J.; Fu, Y.; Zheng, W.; Zhao, Y.; Dang, L.; Stolt, M.J.; Kohler, D.D.; Wang, X.; Czech, K.J.; et al. Single-Crystal Thin Films of Cesium Lead Bromide Perovskite Epitaxially Grown on Metal Oxide Perovskite ($SrTiO_3$). *J. Am. Chem. Soc.* **2017**, 139, 13525.

(2) Song, J.; Li, J.; Li, X.; Xu, L.; Dong, Y.; Zeng, H. Quantum Dot Light-Emitting Diodes Based on Inorganic Perovskite Cesium Lead Halides ($CsPbX_3$). *Adv. Mater.* **2015**, 27, 7162.

(3) Zhang, L.; Yang, X.; Jiang, Q.; Wang, P.; Yin, Z.; Zhang, X.; Tan, H.; Yang, Y.; Wei, M.; Sutherland, B.R.; et al. Ultra-Bright and Highly Efficient Inorganic Based Perovskite Light-Emitting Diodes. *Nat. Commun.* **2017**, 8, 15640.

(4) McMeekin, D.P.; Sadoughi, G.; Rehman, W.; Eperon, G.E.; Saliba, M.; Hörantner, M.T.; Haghighirad, A.; Sakai, N.; Korte, L.; Rech, B.; et al. A Mixed-Cation Lead Mixed-Halide Perovskite Absorber for Tandem Solar Cells. *Science* **2016**, 351, 6269.

(5) Lin, K.; Xing, J.; Quan, L.N.; Pelayo García de Arquer, F.; Gong, X.; Lu, J.; Xie, L.; Zhao, W.; Zhang, D.; Yan, C.; et al. Perovskite Light-Emitting Diodes with External Quantum Efficiency Exceeding 20 Per Cent. *Nature* **2018**, 562, 245.

(6) Li, J.; Du, P.; Li, S.; Liu, J.; Zhu, M.; Tan, Z.; Hu, M.; Luo, J.; Guo, D.; Ma, L.; et al. High-Throughput Combinatorial Optimizations of Perovskite Light-Emitting Diodes Based on All-Vacuum Deposition. *Adv. Funct. Mater.* **2019**, 1903607.

(7) Pan, W.; Yang, B.; Niu, G.; Xue, K.-H.; Du, X.; Yin, L.; Zhang, M.; Wu, H.; Miao, X.-S.; Tang, J. Hot-Pressed $CsPbBr_3$ Quasi-Monocrystalline Film for Sensitive Direct X-ray Detection. *Adv. Mater.* **2019**, 31, 1904405.

(8) Tong, G.; Ono, L.K.; Qi, Y.B. Recent Progress of All-Bromide Inorganic Perovskite Solar Cells. *Energy Technol.* **2019**, 1900961.

(9) Chen, T.; Tong, G.; Xu, E.; Li, H.; Li, P.; Zhu, Z.; Tang, J.; Qi, Y.B.; Jiang, Y. Accelerating Hole Extraction by Inserting 2D Ti_3C_2-MXene Interlayer to All Inorganic Perovskite Solar Cells with Long-Term Stability. *J. Mater. Chem. A* **2019**, 7, 20597.

(10) Stoumpos, C.C.; Malliakas, C.D.; Peters, J.A.; Liu, Z.; Sebastian, M.; Im, J.; Chasapis, T.C.; Wibowo, A.C.; Chung, D.Y.; Freeman, A.J.; et al. Crystal Growth of the Perovskite Semiconductor $CsPbBr_3$: A New Material for High-Energy Radiation Detection. *Cryst. Growth Des.* **2013**, 13, 2722.

(11) Fu, Y.; Zhu, H.; Stoumpos, C.C.; Ding, Q.; Wang, J.; Kanatzidis, M.G.; Zhu, X.; Jin, S. Broad Wavelength Tunable Robust Lasing from Single-Crystal Nanowires of Cesium Lead Halide Perovskites ($CsPbX_3$, X = Cl, Br, I). *ACS Nano* **2016**, 10, 7963.

(12) Eaton, S.W.; Lai, M.; Gibson, N.A.; Wong, A.B.; Dou, L.; Ma, J.; Wang, L.-W.; Leone, S.R.; Yang, P. Lasing in Robust Cesium Lead Halide Perovskite Nanowires. *P.N.A.S.* **2016**, 113, 8, 1993.

(13) Dou, L.; Lai, M.; Kley, C.S.; Yang, Y.; Bischak, C.G.; Zhang, D.; Eaton, S.W.; Ginsberg, N.S.; Yang, P. Spatially Resolved Multicolor $CsPbX_3$ Nanowire Heterojunctions *via* Anion Exchange. *P.N.A.S.* **2017**, 114, 28, 7216.

(14) Oksenberg, E.; Sanders, E.; Popovitz-Biro, R.; Houben, L.; Joselevich, E. Surface-Guided $CsPbBr_3$ Perovskite Nanowires on Flat and Faceted Sapphire with Size-Dependent Photoluminescence and Fast Photoconductive Response. *Nano Lett.* **2018**, 18, 424.

(15) Shoaib, M.; Zhang, X.; Wang, X.; Zhou, H.; Xu, T.; Wang, X.; Hu, X.; Liu, H.; Fan, X.; Zheng, W.; et al. Directional Growth of Ultralong $CsPbBr_3$ Perovskite Nanowires for High-Performance Photodetectors. *J. Am. Chem. Soc.* **2017**, 139, 15592.

(16) Lou, S.; Xuan, T.; Yu, C.; Cao, M.; Xia, C.; Wang, J.; Li, H. Nanocomposites of $CsPbBr_3$ Perovskite Nanocrystals in an Ammonium Bromide Framework with Enhanced Stability. *J. Mater. Chem. C* **2017**, 5, 7431.

(17) Li, C.; Zang, Z.; Chen, W.; Hu, Z.; Tang, X.; Hu, W.; Sun, K.; Liu, X.; Chen, W. Highly Pure Green Light Emission of Perovskite $CsPbBr_3$ Quantum Dots and Their Application for Green Light-Emitting Diodes. *Opt. Express* **2016**, 24, 15071.

(18) Jiang, M.; Hu, Z.; Liu, Z.; Wu, Z.; Ono, L.K.; Qi; Y.B.; Engineering Green-to-Blue Emitting $CsPbBr_3$ Quantum-Dot Films with Efficient Ligand Passivation. *ACS Energy Lett.* **2019**, 4, 2731.

(19) Song, L.; Guo, X.; Hu, Y.; Lv, Y.; Lin, J.; Fan, Y.; Zhang, N.; Liu, X. Improved Performance of $CsPbBr_3$ Perovskite Light-Emitting Devices by Both Boundary and Interface Defects Passivation. *Nanoscale* **2018**, 10, 18315.

(20) Liu, X.; Guo, X.; Lv, Y.; Hu, Y.; Fan, Y.; Lin, J.; Liu, X.; Liu, X. High Brightness and Enhanced Stability of $CsPbBr_3$-Based Perovskite Light-Emitting Diodes by Morphology and Interface Engineering. *Adv. Optical Mater.* **2018**, 6, 1801245.

(21) Endres, J.; Kulbak, M.; Zhao, L.; Rand, B.P.; Cahen, D.; Hodes, G.; Kahn, A. Electronic Sructure of the $CsPbBr_3$/Polytriarylamine (PTAA) System. *J. Appl. Phys.* **2017**, 121, 035304.

(22) Qian, C.-X.; Deng, Z.-Y.; Yang, K.; Feng, J.; Wang, M.-Z.; Yang, Z.; Liu, S.; Feng, H.-J. Interface Engineering of $CsPbBr_3/TiO_2$ Heterostructure with Enhanced Optoelectronic Properties for All-Inorganic Perovskite Solar Cells. *Appl. Phys. Lett.* **2018**, 112, 093901.

(23) Thind, A.S.; Luo, G.; Hachtel, J.A.; Morrell, M.V.; Cho, S.B.; Borisevich, A.Y.; Idrobo, J.-C.; Xing, Y.; Mishra, R. Atomic Structure and Electrical Activity of Grain Boundaries and Ruddlesden-Popper Faults in Cesium Lead Bromide Perovskite. *Adv. Mater.* **2018**, 1805047.

(24) Ohmann, R.; Ono, L.K.; Kim, H.-S.; Lin, H.; Lee, M.V.; Li, Y.; Park, N.-G.; Qi, Y.B. Real-Space Imaging of the Atomic Structure of Organic-Inorganic perovskite. *J. Am. Chem. Soc.* **2015**, 137, 16049.

(25) Hieulle, J.; Stecker, C.; Ohmann, R.; Ono, L.K.; Qi, Y.B. Scanning Probe Microscopy Applied to Organic-Inorganic Halide Perovskite Materials and Solar Cells. *Small Methods* **2018**, 2, 1700295.

(26) She, L.; Liu, M.; Zhong, D. Atomic Structures of $CH_3NH_3PbI_3$(001) Surfaces. *ACS Nano* **2016**, 10, 1126.

(27) Stecker, C.; Liu, K.; Hieulle, J.; Ohmann, R.; Liu, Z.; Ono, L.K.; Wang, G.; Qi, Y.B. Surface Defect Dynamics in Organic−Inorganic Hybrid Perovskites: From Mechanism to Interfacial Properties. *ACS Nano* **2019**, 13, 12127.

(28) Kulbak, M.; Cahen, D.; Hodes, G. How Important Is the Organic Part of Lead Halide Perovskite Photovoltaic Cells? Efficient $CsPbBr_3$ Cells. *J. Phys. Chem. Lett.* **2015**, 6, 2452.

(29) Endres, J.; Egger, D.A.; Kulbak, M.; Kerner, R.A.; Zhao, L.; Silver, S.H.; Hodes, G.; Rand, B.P.; Cahen, D.; Kronik, L.; et al. Valence and Conduction Band Densities of States of Metal Halide Perovskites: A Combined Experimental-Theoretical Study. *J. Phys. Chem. Lett.* **2016**, 7, 2722.

(30) Olthof, S.; Meerholz, K.; Substrate-Dependent Electronic Structure and Film Formation of $MAPbI_3$ Perovskites. *Sci. Rep.* **2017**, 7, 40267.

(31) Hieulle, J.; Wang, X.; Stecker, C.; Son, D.-Y.; Qiu, L.; Ohmann, R.; Ono, L.K.; Mugarza, A.; Yan, Y.; Qi, Y.B. Unraveling the Impact of Halide Mixing on Perovskite Stability. *J. Am. Chem. Soc.* **2019**, 141, 3515.

(32) Choi, J. I. J.; Khan, M. E.; Hawash, Z.; Kim, K. J.; Lee, H.; Ono, L. K.; Qi, Y. B.; Kim, Y.-H.; Park, J. Y. Atomic-Scale view of Stability and Degradation of Single-Crystal $MAPbBr_3$ Surfaces. *J. Mater. Chem. A* **2019**, *7*, 20760.